



PERGAMON

Deep-Sea Research II 49 (2002) 1601–1622

DEEP-SEA RESEARCH
PART II

www.elsevier.com/locate/dsr2

Global sea–air CO₂ flux based on climatological surface ocean pCO₂, and seasonal biological and temperature effects

Taro Takahashi^{a,*}, Stewart C. Sutherland^a, Colm Sweeney^a, Alain Poisson^b,
Nicolas Metz^b, Bronte Tilbrook^c, Nicolas Bates^d, Rik Wanninkhof^e,
Richard A. Feely^f, Christopher Sabine^f, Jon Olafsson^g, Yukihiko Nojiri^h

^a Lamont-Doherty Earth Observatory of Columbia University, Palisades, NY 10964, USA

^b Laboratoire de Biogéochimie et Chimie Marines, Université Pierre et Marie Curie, Case 134 4 place Jussieu,
75252 Paris Cedex 05, France

^c Antarctic CRC and CSIRO Marine Research, Hobart, Tasmania 7001, Australia

^d Bermuda Biological Station for Research, Ferry Reach GE 01, Bermuda

^e AOML, National Oceanographic and Atmospheric Administration, 4301 Rickenbacker Causeway, Miami, FL 33149, USA

^f PMEL, National Oceanographic and Atmospheric Administration, 7600 Sand Point Way, NE, Seattle, WA 98115, USA

^g University of Iceland and Marine Research Institute, Skulagata 4, 121, Reykjavik, Iceland

^h Global Warming Mechanism Laboratory, National Institute for Environmental Studies, Tsukuba, Ibaraki 305-0053, Japan

Abstract

Based on about 940,000 measurements of surface-water pCO₂ obtained since the International Geophysical Year of 1956–59, the climatological, monthly distribution of pCO₂ in the global surface waters representing mean non-El Niño conditions has been obtained with a spatial resolution of 4° × 5° for a reference year 1995. The monthly and annual net sea–air CO₂ flux has been computed using the NCEP/NCAR 41-year mean monthly wind speeds. An annual net uptake flux of CO₂ by the global oceans has been estimated to be 2.2 (+22% or –19%) Pg C yr⁻¹ using the (wind speed)² dependence of the CO₂ gas transfer velocity of Wanninkhof (J. Geophys. Res. 97 (1992) 7373). The errors associated with the wind-speed variation have been estimated using one standard deviation (about ±2 m s⁻¹) from the mean monthly wind speed observed over each 4° × 5° pixel area of the global oceans. The new global uptake flux obtained with the Wanninkhof (wind speed)² dependence is compared with those obtained previously using a smaller number of measurements, about 250,000 and 550,000, respectively, and are found to be consistent within ±0.2 Pg C yr⁻¹. This estimate for the global ocean uptake flux is consistent with the values of 2.0 ± 0.6 Pg C yr⁻¹ estimated on the basis of the observed changes in the atmospheric CO₂ and oxygen concentrations during the 1990s (Nature 381 (1996) 218; Science 287 (2000) 2467). However, if the (wind speed)³ dependence of Wanninkhof and McGillis (Res. Lett. 26 (1999) 1889) is used instead, the annual ocean uptake as well as the sensitivity to wind-speed variability is increased by about 70%.

A zone between 40° and 60° latitudes in both the northern and southern hemispheres is found to be a major sink for atmospheric CO₂. In these areas, poleward-flowing warm waters meet and mix with the cold subpolar waters rich in nutrients. The pCO₂ in the surface water is decreased by the cooling effect on warm waters and by the biological drawdown of pCO₂ in subpolar waters. High wind speeds over these low pCO₂ waters increase the CO₂ uptake rate by the ocean waters.

*Corresponding author. Fax: +1-845-365-2312.

E-mail address: taka@lamont.ldeo.columbia.edu (T. Takahashi).

The $p\text{CO}_2$ in surface waters of the global oceans varies seasonally over a wide range of about 60% above and below the current atmospheric $p\text{CO}_2$ level of about $360 \mu\text{atm}$. A global map showing the seasonal amplitude of surface-water $p\text{CO}_2$ is presented. The effect of biological utilization of CO_2 is differentiated from that of seasonal temperature changes using seasonal temperature data. The seasonal amplitude of surface-water $p\text{CO}_2$ in high-latitude waters located poleward of about 40° latitude and in the equatorial zone is dominated by the biology effect, whereas that in the temperate gyre regions is dominated by the temperature effect. These effects are about 6 months out of phase. Accordingly, along the boundaries between these two regimes, they tend to cancel each other, forming a zone of small $p\text{CO}_2$ amplitude. In the oligotrophic waters of the northern and southern temperate gyres, the biology effect is about $35 \mu\text{atm}$ on average. This is consistent with the biological export flux estimated by Laws et al. (*Glob. Biogeochem. Cycles* 14 (2000) 1231). Small areas such as the northwestern Arabian Sea and the eastern equatorial Pacific, where seasonal upwelling occurs, exhibit intense seasonal changes in $p\text{CO}_2$ due to the biological drawdown of CO_2 . © 2002 Published by Elsevier Science Ltd.

Résumé

Une distribution climatologique mensuelle moyenne de $p\text{CO}_2$ de surface de l'océan mondial a été établie pour l'année 1995 (pour les années sans El Niño) à partir de 940.000 mesures dans les eaux de surface, acquises depuis l'Année Géophysique Internationale (1956–59), avec une résolution spatiale de $4^\circ \times 5^\circ$. Les flux de CO_2 air-mer ont été ensuite calculés, à l'échelle mensuelle et annuelle, en utilisant la distribution des vents mensuels du NCEP/NCAR moyennés sur 41 ans. Le flux net océanique global de CO_2 a été estimé à un puits de $2.2 (+22\% \text{ ou } -19\%) \text{ Pg C an}^{-1}$ en utilisant l'équation de Wanninkhof (*Geophys. Res.* 97 (1992) 7373) dans laquelle le coefficient de transfert (ou la vitesse de piston) du CO_2 est exprimé en fonction du carré de la vitesse du vent; les incertitudes associées à la vitesse du vent ont été calculées en utilisant une erreur standard de $\pm 2 \text{ m s}^{-1}$ pour un vent moyen observé sur chaque pixel de $4^\circ \times 5^\circ$ de l'océan global. Le nouveau flux global ainsi calculé (carré de la vitesse du vent dans le coefficient de transfert) est à 0.2 Pg C an^{-1} près, en accord avec nos estimations antérieures basées respectivement sur 250.000 et 550.000 mesures seulement. Ce résultat est également compatible avec les estimations de $2.0 \pm 0.6 \text{ Pg C an}^{-1}$ de Keeling et al. (*Nature* 381 (1996) 218) et de Battle et al. (*Science* 287 (2000) 2467) basées sur la variation des teneurs en CO_2 et oxygène atmosphériques pendant la décennie des années 90. Cependant l'utilisation de l'équation de Wanninkhof et McGillis (*Res. Lett.* 26 (1999) 1889), faisant intervenir le coefficient de transfert de CO_2 exprimé en fonction du cube de la vitesse du vent, donne des valeurs du flux annuel global ainsi que la sensibilité à la variation de la vitesse du vent plus élevées de 70%.

Le puits majeur de CO_2 atmosphérique est situé dans la bande de latitude comprise entre 40 et 60° pour les deux hémisphères, où les eaux chaudes se dirigeant vers le pôle convergent et se mélangent avec des eaux froides subpolaires riches en sels nutritifs. La diminution de $p\text{CO}_2$ des eaux de surface subpolaires est due à la fois à leur refroidissement et à la pompe biologique. L'intensité des vents dans ces régions où $p\text{CO}_2$ est faible en surface intensifie encore le pompage de CO_2 .

La variation saisonnière de $p\text{CO}_2$ dans les eaux de surface de l'océan global peut atteindre $\pm 60\%$ de la valeur actuelle de $p\text{CO}_2$ atmosphérique moyen ($360 \mu\text{atm}$). Une carte de l'amplitude de la variation saisonnière de $p\text{CO}_2$ dans les eaux de surface ainsi que l'effet de l'utilisation du CO_2 par la production biologique et l'influence de la variation saisonnière de la température (estimée en utilisant des données saisonnières de température) sont présentées séparément. La variation saisonnière de $p\text{CO}_2$ des eaux de surface situées entre les pôles et environ 40° et celles des régions équatoriales est principalement due à l'effet de la pompe biologique, alors que dans les tourbillons des régions centrales c'est l'effet thermique qui domine, ces deux effets étant déphasés d'environ 6 mois. En conséquence, dans les régions frontières de ces deux zones les effets thermique et biologique se compensent, ce qui engendre des variations saisonnières de $p\text{CO}_2$ de faible amplitude. Dans les eaux oligotrophes des tourbillons centraux des régions tempérées, l'influence de la biologie est estimé à $35 \mu\text{atm}$ en moyenne, ce qui est compatible avec le flux biologique exporté estimé par Laws et al. (*Glob. Biogeochem. Cycles* 14 (2000) 1231). L'importance de l'effet biologique sur $p\text{CO}_2$ dû à l'intensité des remontées saisonnières d'eaux a été mis en évidence dans des régions de surface limitées du nord-ouest de la mer d'Arabie et du Pacifique est-équatorial.

1. Introduction

The difference between the $p\text{CO}_2$ in the surface ocean water and that in the overlying air represents the thermodynamic driving potential for the CO_2 gas transfer across the sea surface. The direction of the net transfer of CO_2 is governed by the $p\text{CO}_2$ differences, and the magnitude of the net sea–air CO_2 flux may be expressed as a product of the $p\text{CO}_2$ difference and the sea–air CO_2 gas transfer velocity, which may be parameterized as a function of wind speed. The flux values thus estimated depend on the wind field used and the formulation for the wind-speed dependence on the gas transfer velocity. In this paper, we will present a set of the climatological monthly distribution field of surface-water $p\text{CO}_2$ over the global oceans, which has been improved using an expanded data set consisting of about 940,000 $p\text{CO}_2$ measurements. The effects of wind fields and the wind-speed dependence for the gas transfer velocity on the estimated CO_2 flux will be discussed using the NCEP/NCAR wind-speed data averaged over 41 years and the single year data for 1995.

Over the global oceans, the seasonal and geographical variation of surface-water $p\text{CO}_2$ is much greater than that of atmospheric $p\text{CO}_2$, and hence the direction and magnitude of the sea–air CO_2 transfer flux are mainly regulated by the oceanic $p\text{CO}_2$. The $p\text{CO}_2$ in surface-ocean water is known to vary geographically and seasonally over a wide range between about 150 and 550 μatm , about 60% below and above the mean atmospheric $p\text{CO}_2$ of about 360 μatm (or about 370 ppm mole fraction in dry air) in the year 2000. The $p\text{CO}_2$ in mixed-layer water that exchanges CO_2 directly with the atmosphere is affected by seasonal changes in temperature, total CO_2 concentration, and alkalinity. While the water temperature is primarily regulated by physical processes (i.e. solar energy input, sea–air heat exchanges, and mixed-layer thickness), the latter two are primarily controlled by biological processes (i.e. photosynthesis, respiration and calcification) and by upwelling of subsurface waters enriched in respired CO_2 and nutrients. We present a method for distinguishing the seasonal biological effect on surface-water $p\text{CO}_2$ from the effect of

seasonal temperature changes, and discuss the relative significance of these effects in different regions of the global oceans.

2. Climatological distribution of surface-water $p\text{CO}_2$

2.1. Database

The climatological distribution of the surface-water $p\text{CO}_2$ for each month over the global oceans has been computed using about 940,000 measurements for $p\text{CO}_2$ in surface waters made since the International Geophysical Year, 1956–59. The size of our present database has been increased from about 250,000 used in Takahashi et al. (1997) to about 550,000 used in Takahashi et al. (1999) and then to the present size. The data source prior to 1996 is described in Takahashi et al. (1997). The newer data sets used in this study include Sabine et al. (1997), Bates et al. (1998), Bates (2001), Feely et al. (1999), Metzl et al. (1995, 1999), Murphy et al. (1998), Nojiri, (2001a, b), Rubin et al. (1998), Rubin (2000), Sabine and Key (1998), Sabine et al. (1997, 1999, 2000), Sweeney (2000), Sweeney et al. (2000a, b), Takahashi and Goddard (1998), Takahashi et al. (2000), and the data files assembled at the laboratories of the authors of this paper.

2.2. Computational method

The space–time interpolation method used for this paper is based on the scheme developed by Takahashi et al. (1993). However, since a number of improvements have been made, the methods of data selection and changes in the computational procedures will be explained briefly below.

First, since $p\text{CO}_2$ in the equatorial Pacific surface waters changes drastically during El Niño periods, the observations made in the equatorial Pacific between 10°N and 10°S during El Niño events have been excluded from the data set. Thus, the results shown in this paper represent the climatological distributions under non-El Niño conditions.

Second, since the surface-water $p\text{CO}_2$ has been changing with time in response to the atmospheric

$p\text{CO}_2$ increase, the measurements made in different years need to be corrected to a single reference year (arbitrarily chosen to be 1995) on the basis of the following two lines of evidence:

(a) Surface waters in subtropical gyres mix vertically at slow rates with subsurface waters due to the presence of strong stratification at the base of the winter-mixed layer. This results in a long contact time with the atmosphere to exchange CO_2 . Therefore, the $p\text{CO}_2$ in these warm waters follows the increasing trend of atmospheric CO_2 as demonstrated by Inoue et al. (1995), Feely et al. (1999), and Bates (2001). Accordingly, the $p\text{CO}_2$ measured in a given month and year is corrected to the same month of the reference year 1995 using changes in the atmospheric CO_2 concentration occurred during this period. Oceanic $p\text{CO}_2$ measurements made after the beginning of 1979 have been corrected to 1995 using the atmospheric CO_2 concentration data from the GLOBALVIEW-CO2 database (2000), in which the zonal mean atmospheric concentrations (for each 0.05 in sine of latitude) within the planetary boundary layer are summarized for each month since 1979–2000. Pre-1979 oceanic $p\text{CO}_2$ data were corrected to 1979 using the annual mean trend for the global mean atmospheric CO_2 concentration constructed from the Mauna Loa data of Keeling and Whorf (2000), and then from 1979 to 1995 using the GLOBALVIEW-CO2 database. Measurements for $p\text{CO}_2$ made in the following areas have been corrected for the time of observation; 45°N–50°S in the Atlantic Ocean, north of 50°S in the Indian Ocean, 40°N–50°S in the western Pacific west of the date line, and 40°N–60°S in the eastern Pacific east of the date line.

(b) In contrast to subtropical gyres, surface waters in high-latitude regions are mixed convectively with deep waters during the fall–winter seasons, and their CO_2 properties tend to remain unchanged from year to year, reflecting those of deep waters in which the effect of increased atmospheric CO_2 is diluted to undetectable levels as observed by Takahashi et al. (1997). Hence, no correction is necessary for the year of measurements.

These $p\text{CO}_2$ values adjusted to the reference year 1995 are binned into each of 750,000 pixels

[=(72 pixels along the E–W direction) × (41 along the N–S direction) × (365 days)], which represent the global 4° × 5° grid for each day in a single virtual calendar year. Since $p\text{CO}_2$ measurements have been made only sparsely in each year, it is necessary to pool the data collected over 40 years into a single reference year in order to have a sufficient spatial and seasonal coverage over the global oceans.

On the basis of the database thus assembled, mean monthly global distributions of $p\text{CO}_2$ have been constructed using an interpolation method based on a lateral 2-dimensional advection–diffusion transport equation for surface-ocean water (Takahashi et al., 1995, 1997). The monthly field for lateral advection of global surface ocean waters obtained by Toggweiler et al. (1989) is used and, for the lateral diffusive transport, a constant value of 2000 m² s⁻¹ (Thiele et al., 1986; Jenkins, 1991) is used. The equation is solved iteratively using a finite-difference algorithm with a time step of 1 day through the reference year 1995. The computational domains are joined at December 31, 1995, with January 1, 1995, and along the prime meridian to ensure continuity in time and space. Typically, several thousand iterations are necessary before solutions are converged. The solutions thus obtained give surface-water $p\text{CO}_2$ values for 4° × 5° pixels where no observations exist, while the observed values are explicitly satisfied. Although the solutions give daily distributions, monthly mean distributions for the surface-water $p\text{CO}_2$ have been computed and are presented in Fig. 1. It should be pointed out that in the earlier papers (Takahashi et al., 1997, 1999), the sea–air $p\text{CO}_2$ difference, $\Delta p\text{CO}_2$, was interpolated, instead of seawater $p\text{CO}_2$, using the transport equation for surface ocean waters. This assumes implicitly that atmospheric CO_2 in the overlying air was transported in the same manner as surface-ocean waters. However, this does not represent the actual transport of the atmosphere correctly. Hence, in the present work, we applied the ocean-transport equation for interpolating surface-ocean $p\text{CO}_2$ data.

In order to test the validity of our interpolation scheme, we computed monthly temperature fields for the world oceans using water temperature

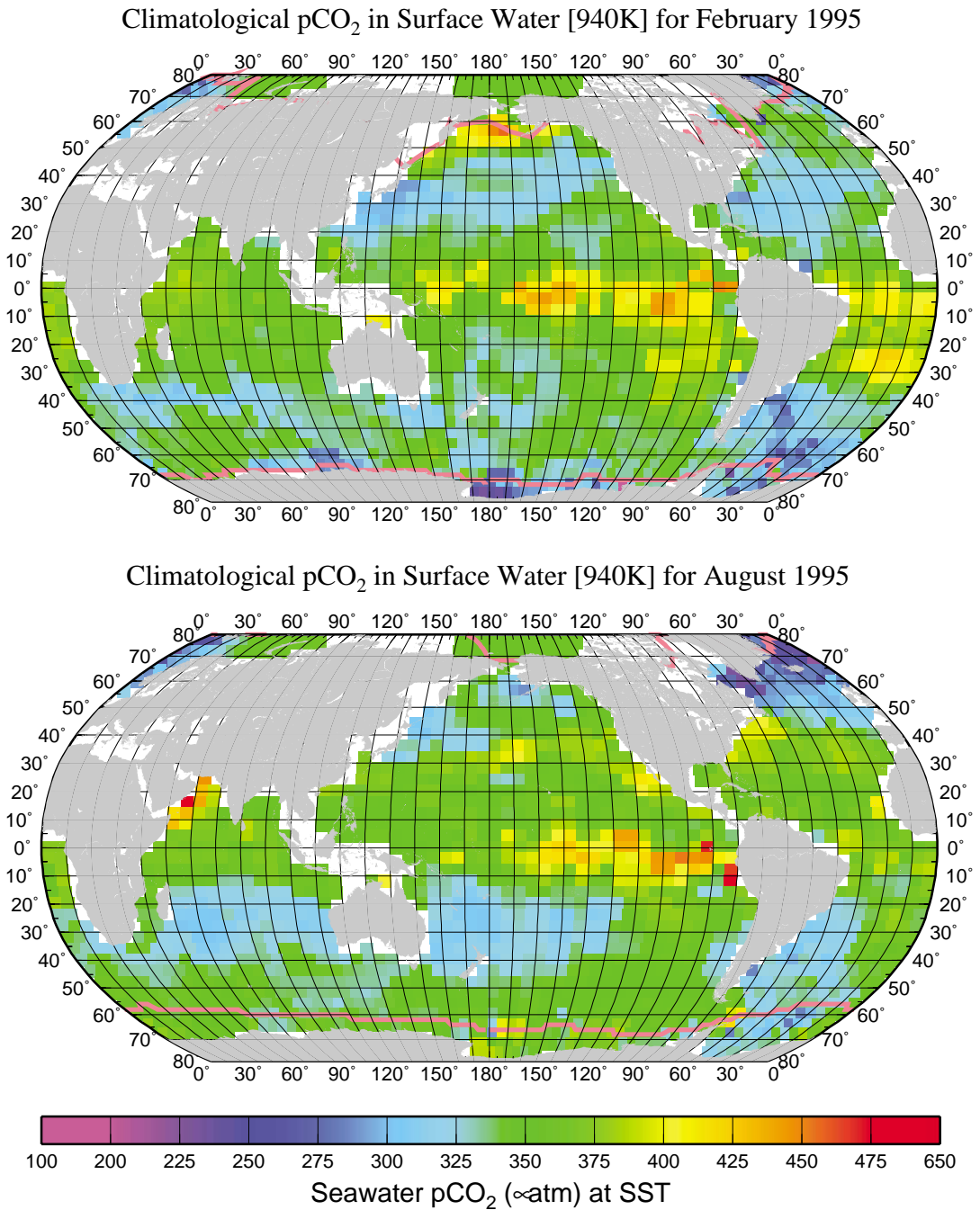


Fig. 1. Climatological mean distribution of surface-water $p\text{CO}_2$ in February (top) and August (bottom) in the reference year 1995.

values observed concurrently with $p\text{CO}_2$ in surface waters, and compared them with the climatological mean monthly SST fields given in the World

Ocean Database (1998). For the observed 8938 monthly pixels, the mean difference between our pixel values and the World Ocean Database values

is $-0.05 \pm 1.40^\circ\text{C}$; and for the observed and interpolated 21,108 monthly pixels, the mean difference is $0.28 \pm 1.64^\circ\text{C}$. The mean difference for the interpolated global SST field includes zero well within one standard deviation. The mean difference of -0.05°C for the observed pixels suggests that our $p\text{CO}_2$ observations represent distributions consistent with the climatological SST values. However, if 0.28°C is taken as a measure for a systematic error introduced by imperfections of our interpolation scheme, it should correspond to an error of $\pm 3 \mu\text{atm}$ in seawater $p\text{CO}_2$, on the basis that the seasonal temperature effect on ocean-surface-water $p\text{CO}_2$ is in a range between $+4$ and $-4\% \text{ }^\circ\text{C}^{-1}$ over the global oceans (Takahashi et al., 1993). While the temperature effect on $p\text{CO}_2$ in isochemical conditions ($\partial \ln p\text{CO}_2 / \partial T$) is $+4.23\% \text{ }^\circ\text{C}^{-1}$ (Takahashi et al., 1993), the temperature dependence changes over the range indicated above because seasonal temperature changes in mixed-layer water are accompanied with an increase (by deep-water upwelling and sea–air CO_2 exchange) or decrease (by photosynthesis and sea–air CO_2 exchange) in the total CO_2 concentration.

2.3. Distribution of surface-water $p\text{CO}_2$

The mean monthly $p\text{CO}_2$ values in August and February for the reference year 1995 are shown in Fig. 1 as examples of the 12 monthly distributions obtained. These monthly distributions represent climatological mean distributions for non-El Niño conditions based on measurements of surface-water $p\text{CO}_2$ made from 1958 through 2000.

Fig. 1 shows that low $p\text{CO}_2$ areas (blue and purple) are found in the high-latitude areas in the Southern Ocean during the austral summer (February, the upper panel) and in the subarctic and arctic Atlantic Ocean during the northern summer (August, the lower panel). These areas represent an intense sink for atmospheric CO_2 , which is attributed primarily to the photosynthetic utilization of CO_2 . The broad low $p\text{CO}_2$ areas (dark and light blue) which are found in the mid-latitude areas of the North Pacific and North Atlantic during the northern winter

(February, the upper panel), are due primarily to the cooling of the warm Kuroshio and Gulf Stream waters, respectively, as they flow to higher latitudes. Similar features are found in the mid-latitude areas of the southern hemisphere oceans during the austral winter (August, the lower panel). The high $p\text{CO}_2$ values (yellow and red) observed in the eastern equatorial Pacific are a product of local upwelling of CO_2 -rich waters along the equator and advection of CO_2 -enriched waters from the South American coast (Feely et al., 1999; Etcheto et al., 1999). The $p\text{CO}_2$ value in the equatorial zone of the Pacific decreases from east to west as a result of biological utilization of CO_2 , reduced upwelling, and loss of CO_2 to air by air–sea gas exchange (Quay, 1987). High $p\text{CO}_2$ values are also observed in the subarctic northwestern Pacific during the northern winter (February, the upper panel) and in the Arabian Sea during the northern summer (the lower panel). The former is attributed to the convective mixing of subsurface waters in the subarctic Pacific during winter, and the latter to the monsoon-induced upwelling in the Arabian Sea during summer.

3. Net sea–air CO_2 flux

3.1. Computational method

Net sea–air CO_2 flux, F , can be estimated using: $F = k \cdot \alpha \cdot (\Delta p\text{CO}_2)_{\text{sea–air}}$, where k is the CO_2 gas transfer velocity, α is the solubility of CO_2 in seawater (Weiss, 1974), and $(\Delta p\text{CO}_2)_{\text{sea–air}}$ is the sea–air $p\text{CO}_2$ difference. The sea–air $p\text{CO}_2$ difference is computed using the mean monthly $p\text{CO}_2$ values in surface waters obtained in this study and the atmospheric $p\text{CO}_2$ computed using the zonal mean CO_2 concentrations in the dry atmosphere for 1995 reported by the GLOBALVIEW-CO2 (2000). The climatological mean barometric pressure (P_b) (Atlas of Surface Marine Data, 1994) and equilibrium water vapor pressure (P_w) at climatological surface water temperature and salinity (World Ocean Database, 1998) are used for computing the atmospheric $p\text{CO}_2$ in the

relationship

$$(p\text{CO}_2)_{\text{air}} = (\text{CO}_2 \text{ conc.})_{\text{air}}(P_b - P_w).$$

3.2. Global distribution of the net sea–air CO₂ flux

Table 1 shows the results of net sea–air CO₂ flux computed for regional and global oceans using the

CO₂ gas transfer velocity vs. wind-speed relation formulated by Wanninkhof (1992) and the NCEP-41-year mean monthly wind speed over each pixel area. The results of earlier studies (Takahashi et al., 1997, 1999) have been corrected using the same wind speeds and the Wanninkhof (1992) relationship. Although the number of *p*CO₂ measurements in the database has increased from about 250,000

Table 1

The net sea–air CO₂ flux computed using the climatological sea–air *p*CO₂ difference, and the NCEP/NCAR 41-year mean monthly wind speed and the wind speed dependence of CO₂ gas transfer velocity by Wanninkhof (1992; named W92 in the table)

Lat. band	$\Delta p\text{CO}_2$ data	Gas trans./ wind data	Pacific Ocean (Pg C yr ⁻¹)	Atlantic Ocean (Pg C yr ⁻¹)	Indian Ocean (Pg C yr ⁻¹)	Southern Ocean (Pg C yr ⁻¹)	Global Ocean (Pg C yr ⁻¹)
<i>N of 50°N</i>	This work	W92/41-yr	+0.01	-0.40	—	—	-0.39
	T99	W92/41-yr	-0.02	-0.48	—	—	-0.49
	T97	W92/41-yr	+0.01	-0.48	—	—	-0.47
<i>14°N–50°N</i>	This work	W92/41-yr	-0.64	-0.34	+0.07	—	-0.92
	T99	W92/41-yr	-0.62	-0.32	+0.06	—	-0.87
	T97	W92/41-yr	-0.55	-0.37	+0.05	—	-0.87
<i>14°N–14°S</i>	This work	W92/41-yr	+0.74	+0.15	+0.18	—	+1.07
	T99	W92/41-yr	+0.73	+0.18	+0.15	—	+1.06
	T97	W92/41-yr	+0.78	+0.15	+0.18	—	+1.11
<i>14°S–50°S</i>	This work	W92/41-yr	-0.51	-0.33	-0.67	—	-1.51
	T99	W92/41-yr	-0.48	-0.27	-0.79	—	-1.54
	T97	W92/41-yr	-0.46	-0.29	-0.57	—	-1.32
<i>S of 50°S</i>	This work	W92/41-yr	—	—	—	-0.47	-0.47
	T99	W92/41-yr	—	—	—	-0.59	-0.59
	T97	W92/41-yr	—	—	—	-0.42	-0.42
	—	—	—	—	—	—	—
<i>Oceanic Regions</i>	This work	W92/41-yr	-0.40	-0.92	-0.43	-0.47	-2.22
	T99	W92/41-yr	-0.39	-0.88	-0.58	-0.59	-2.44
	T97	W92/41-yr	-0.22	-0.99	-0.34	-0.42	-1.97
<i>Regional Flux (%)</i>	This work	W92/41-yr	18	41	19	21	100
	T99	W92/41-yr	16	36	24	24	100
	T97	W92/41-yr	12	50	17	21	100
<i>Areas</i>	(10 ⁶ km ²)	—	151.6	72.7	53.2	31.7	309.1
	(%)	—	49.0	23.5	17.2	10.2	100

The fluxes reported by Takahashi et al. (1999; named T99) and Takahashi et al. (1997; named T97) have been corrected using the NCEP/NCAR 41-year mean monthly wind speeds over each 4° × 5° pixel area (named 41-yr). The sea–air *p*CO₂ difference, $\Delta p\text{CO}_2$, used in this work is based on about 940,000 surface water *p*CO₂ measurements corrected to the reference year 1995; that in T99 is based on about 550,000 surface water *p*CO₂ measurements corrected to the reference year 1995; and that in T97 is based on about 250,000 measurements corrected to 1990. See text for the interpolation method used in T97 and T99

for the 1997 study to about 550,000 for the 1999 study and then to 940,000 for this study, the regional net sea–air $p\text{CO}_2$ flux values are found to be consistent within $\pm 10\%$ on the average. The global fluxes are also mutually consistent within about $\pm 10\%$ yielding $2.2 \pm 0.2 \text{ Pg C yr}^{-1}$ for the 1995 global ocean flux. This suggests that the global $p\text{CO}_2$ fields estimated using these three database sizes are consistent with each other to within $\pm 10\%$. The global sea–air CO_2 flux is consistent with the estimate of $2.0 \pm 0.6 \text{ Pg C yr}^{-1}$ obtained on the basis of the changes of the atmospheric oxygen and CO_2 concentrations observed during the 1990s (Keeling et al., 1996; Battle et al., 2000). A number of model studies (e.g., Sarmiento et al., 1992; Siegenthaler and Sarmiento, 1993; Joos and Bruno, 1998) yield a mean global ocean uptake of about 2 Pg C yr^{-1} .

The flux estimates presented in Table 1 are supported by the results from these two independent lines of investigations.

Fig. 2 shows the distribution of the mean annual net sea–air CO_2 flux. The eastern equatorial Pacific and the northwestern Arabian Sea are the most intense CO_2 source areas (red–orange). The tropical Atlantic and Indian Oceans and the northwestern subarctic Pacific are also prominent source areas. Strong sink areas are found in the transition zone between the subtropical gyre and subpolar waters, i.e. 40°N – 60°N and 40°S – 60°S . In these areas, low $p\text{CO}_2$ waters are formed by the juxtaposition of the cooling of warm waters with the biological drawdown of $p\text{CO}_2$ in the nutrient-rich subpolar waters. High wind speeds over these low $p\text{CO}_2$ waters increase the CO_2 uptake rate by ocean waters. The regional flux (%) values listed

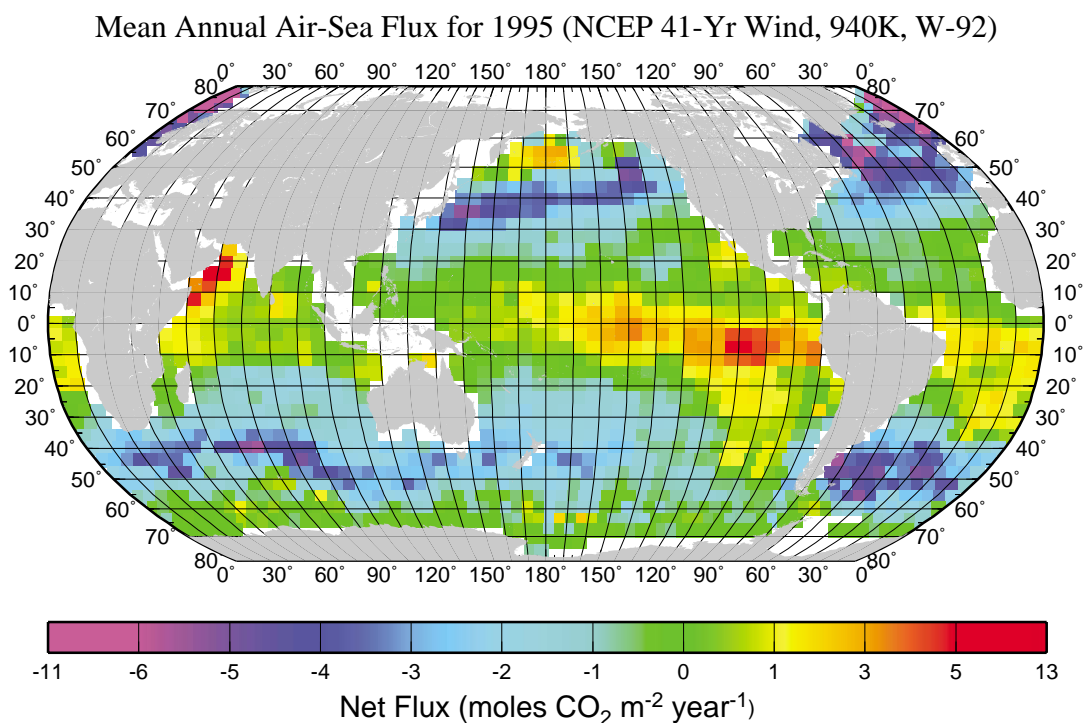


Fig. 2. Mean annual net air–sea flux for CO_2 (mole $\text{CO}_2 \text{ m}^{-2} \text{ yr}^{-1}$) for 1995. The following information has been used; (a) climatological distribution of surface-water $p\text{CO}_2$ for the reference year 1995, (b) the NCEP/NCAR 41-year mean wind speeds, (c) the long-term wind-speed dependence of the sea–air CO_2 transfer velocity by Wanninkhof (1992), (d) the concentration of atmospheric CO_2 in dry air in 1995 (GLOBALVIEW- CO_2 , 2000), and (e) the climatological barometric pressure and sea-surface temperature (Atlas of Surface Marine Data, 1994). Red–yellow areas indicate that the ocean is a source for atmospheric CO_2 , and blue–purple areas indicate that the ocean is a CO_2 sink.

near the bottom of Table 1 indicate that, although the Southern Ocean (south of 50°S) occupies only 10% of the global ocean area, it takes up about 20+ % of the global ocean CO₂ uptake flux. Similarly, the Atlantic Ocean (north of 50°S) occupies about 24% of the ocean area and takes up about 40+ % of the global ocean CO₂ uptake. In contrast, the Pacific Ocean (north of 50°S) takes up only 18% of the global ocean CO₂ uptake, whereas it occupies 49% of the global ocean area. This is due primarily to the fact that the equatorial Pacific is an intense CO₂ source area, and secondarily to the fact that the southeastern South Pacific is a weak CO₂ source area unlike the other oceans. If the CO₂ source flux from the equatorial Pacific is reduced during El Niño events (Feely et al., 1999), then the Pacific as a whole would become a stronger CO₂ sink.

3.3. *Effects of wind speed and gas transfer velocity on the CO₂ flux*

The CO₂ flux thus computed depends sensitively on the choice of the wind speed field and the wind-speed dependence of the CO₂ gas transfer velocity across the sea–air interface. We consider two sets of wind-speed distributions: the climatological mean wind-speed field based on the NCEP/NCAR data collected over the past 41 years, and the NCEP/NCAR annual wind-speed distribution during 1995. These wind data have been re-sampled for our 4° × 5° grid and used to compute mean monthly values for each pixel area. For the CO₂ gas transfer velocity, we use the (wind speed)² dependence of Wanninkhof (1992) (his Eq. (1) for a long-term average wind, named W92) and the (wind speed)³ dependence of Wanninkhof and McGillis (1999) (their Eq. (5) for a long-term average wind, named WM99). Their Rayleigh wind-speed distribution function, which is a solution to the Weibull distribution for isotropic winds, is assumed for both of these equations. The regional and global sea–air CO₂ fluxes computed using four combinations of the transfer velocity formulations and wind-speed fields are summarized in Table 2.

The fluxes computed using the W92 and the NCEP/NCAR 41-year mean wind (named 41-yr)

are listed in the first row for each grouping for zonal bands, Oceanic Regions and Regional Flux (%) in Table 2. The column “Errors in Flux” located at the right extreme of the table lists the deviations from the mean flux that have been computed using one standard deviation in wind speeds (about $\pm 2 \text{ m s}^{-1}$ on the global average) above and below from the mean monthly wind speed in each pixel area. These changes in wind speeds affect the regional and global flux values by about $\pm 25\%$. The fluxes computed using the single year mean wind-speed data for 1995 are listed in the second line in each zonal band group in the table. The wind speeds for 1995 are much lower than the 41-year mean in the northern hemisphere and higher over the Southern Ocean. Accordingly, the northern ocean sink fluxes are less than the climatological mean and the Southern Ocean sink fluxes are stronger. The global mean ocean uptake flux of $-1.8 \text{ Pg C yr}^{-1}$ is about 18% below the climatological mean of $-2.2 \text{ Pg C yr}^{-1}$ and is within $\pm 20\%$ estimated on the basis of the standard deviation of the wind-speed data.

When the (wind speed)³ dependence is used, the CO₂ fluxes in higher-latitude areas with strong winds are increased significantly, as are the errors due to wind-speed variability. The global ocean uptake flux computed with the 41-year mean wind-speed data and the 1995 data is, respectively, -3.7 and $-3.0 \text{ Pg C yr}^{-1}$, an increase by about 70% over the flux that is computed using the (wind speed)² dependence. These flux values are significantly greater than the flux of $-2.0 \pm 0.6 \text{ Pg C yr}^{-1}$ during the 1990s (Keeling et al., 1996; Battle et al., 2000) estimated by the observed changes of the atmospheric CO₂ and oxygen concentrations. However, the relative magnitudes for CO₂ uptake by ocean basins (shown in % in the last four rows in the table) remain nearly unaffected by the choice of the wind-speed dependence of the gas-transfer velocity.

As noted by Wanninkhof et al. (2002), the cubic parameterization for long-term winds used in this study assumes that the regional wind-speed spectrum follows the Rayleigh distribution function. If the regional distributions are determined from the NCEP 6-h wind products, the global flux will decrease to $-3.0 \text{ Pg C yr}^{-1}$ for the

Table 2

The effect of wind speeds and that of the wind-speed dependence of CO₂ gas transfer velocity on the net sea–air CO₂ flux are shown using the climatological sea–air pCO₂ difference obtained in this work

Lat. band	Gas trans./ wind data	Pacific Ocean (Pg C yr ⁻¹)	Atlantic Ocean (Pg C yr ⁻¹)	Indian Ocean (Pg C yr ⁻¹)	Southern Ocean (Pg C yr ⁻¹)	Global Ocean (Pg C yr ⁻¹)	Errors in flux (%)
<i>N of 50°N</i>	W92/41-yr	+0.01	-0.40	—	—	-0.39	+28, -23
	W92/1995	+0.03	-0.18	—	—	-0.14	
	WM99/41-yr	+0.03	-0.55	—	—	-0.52	+44, -35
	WM99/1995	+0.07	-0.17	—	—	-0.10	
<i>14°N-50°N</i>	W92/41-yr	-0.64	-0.34	+0.07	—	-0.92	+25, -23
	W92/1995	-0.29	-0.28	+0.03	—	-0.54	
	WM99/41-yr	-0.94	-0.48	+0.10	—	-1.31	+43, -32
	WM99/1995	-0.29	-0.38	+0.02	—	-0.64	
<i>14°N-14°S</i>	W92/41-yr	+0.74	+0.15	+0.18	—	+1.07	+29, -24
	W92/1995	+0.61	+0.07	+0.15	—	+0.83	
	WM99/41-yr	+0.67	+0.14	+0.20	—	+1.00	+43, -31
	WM99/1995	+0.62	+0.05	+0.12	—	+0.79	
<i>14°S-50°S</i>	W92/41-yr	-0.51	-0.33	-0.67	—	-1.51	+22, -20
	W92/1995	-0.57	-0.31	-0.50	—	-1.38	
	WM99/41-yr	-0.68	-0.51	-0.97	—	-2.16	+37, -30
	WM99/1995	-0.88	-0.51	-0.63	—	-2.02	
<i>S of 50°S</i>	W92/41-yr	—	—	—	-0.47	-0.47	+26, -21
	W92/1995	—	—	—	-0.58	-0.58	
	WM99/41-yr	—	—	—	-0.74	-0.74	+41, -32
	WM99/1995	—	—	—	-1.02	-1.02	
	—	—	—	—	—	—	—
<i>Oceanic Regions</i>	W92/41-yr	-0.40	-0.92	-0.43	-0.47	-2.22	+22, -19
	W92/1995	-0.21	-0.69	-0.33	-0.58	-1.81	
	WM99/41-yr	-0.92	-1.39	-0.67	-0.74	-3.72	+40, -32
	WM99/1995	-0.48	-1.01	-0.48	-1.02	-3.00	
<i>Regional Flux (%)</i>	W92/41-yr	18	41	19	21	100	
	W92/1995	12	38	18	32	100	
	WM99/41-yr	25	37	18	20	100	
	WM99/1995	16	34	16	34	100	

The flux values have been computed using the (wind speed)² dependence of CO₂ gas transfer velocity by Wanninkhof (1992; named W92) and the (wind speed)³ dependence by Wanninkhof and McGillis (1999; named WM99), respectively, for each of the two sets of wind data: the NCEP/NCAR 41-year (named 41-yr in the table) and 1995 mean monthly wind speeds. Errors in flux (% in the flux) listed in the extreme right column represent the flux changes resulting from + or - one standard deviation (about $\pm 2 \text{ m s}^{-1}$ on the global average) from the annual mean wind speed in each pixel area. The positive errors in the flux represent when the mean monthly wind speed over each pixel area was increased by one standard deviation; and the negative errors represent when the mean wind speed was reduced by one standard deviation

NCEP-41-year wind and $-2.3 \text{ Pg C yr}^{-1}$ for the NCEP-1995 wind data. This indicates that the estimated flux values are also sensitive to wind-speed spectra.

4. Seasonal variation of pCO₂ in surface waters

On a global scale, the temperature effect on surface-water pCO₂ is similar in magnitude but

opposite in direction to the biological effect, in which changes of the total CO_2 concentration is the dominant factor. The $p\text{CO}_2$ in surface ocean waters doubles for every 16°C temperature increase ($\partial \ln p\text{CO}_2 / \partial T = 0.0423^\circ\text{C}^{-1}$, Takahashi et al., 1993). For a parcel of seawater with constant chemical composition, its $p\text{CO}_2$ would be increased by a factor of 4 when it is warmed from polar water temperatures of about -1.9°C to equatorial water temperatures of about 30°C . On the other hand, the total CO_2 concentration in surface waters ranges from about $2150 \mu\text{mol kg}^{-1}$ in polar waters to $1850 \mu\text{mol kg}^{-1}$ in tropical waters. If a global mean Revelle factor ($\partial \ln p\text{CO}_2 / \partial \ln \text{TCO}_2$) of 10 is used, this decrease of TCO_2 should cause a reduction of surface-water $p\text{CO}_2$ by a factor of $1/4.5$ ($= (p\text{CO}_2)_{\text{tropical}} / (p\text{CO}_2)_{\text{polar}} = (1850/2150)^{10}$). From the climatological mean monthly $p\text{CO}_2$ data, we can derive the distribution and magnitude of seasonal amplitude of surface-water $p\text{CO}_2$ over the global oceans. The effect of temperature on seasonal amplitude is differentiated from that of the TCO_2 effect, and the relative importance of these processes for regulating the seasonal amplitude in $p\text{CO}_2$ is mapped over the global oceans. This information is important not only for understanding the time-space variability for the sea-air CO_2 exchange, but also for planning future field investigations. Although the maximum level of $p\text{CO}_2$ and the amount of nutrients available for the photosynthesis are governed primarily by the vertical flux of subsurface waters, this flux is difficult to measure due to the lack of widely distributed tracers, and can only be estimated reliably in specific areas such as the Weddell Sea (e.g., Martinson, 1990; Martinson and Iannuzzi, 1998). Therefore, the effect of the vertical flux of deep waters is not addressed in this paper.

4.1. Method of analysis and examples

The method used for the analysis will be illustrated using seasonal data observed at three contrasting locations.

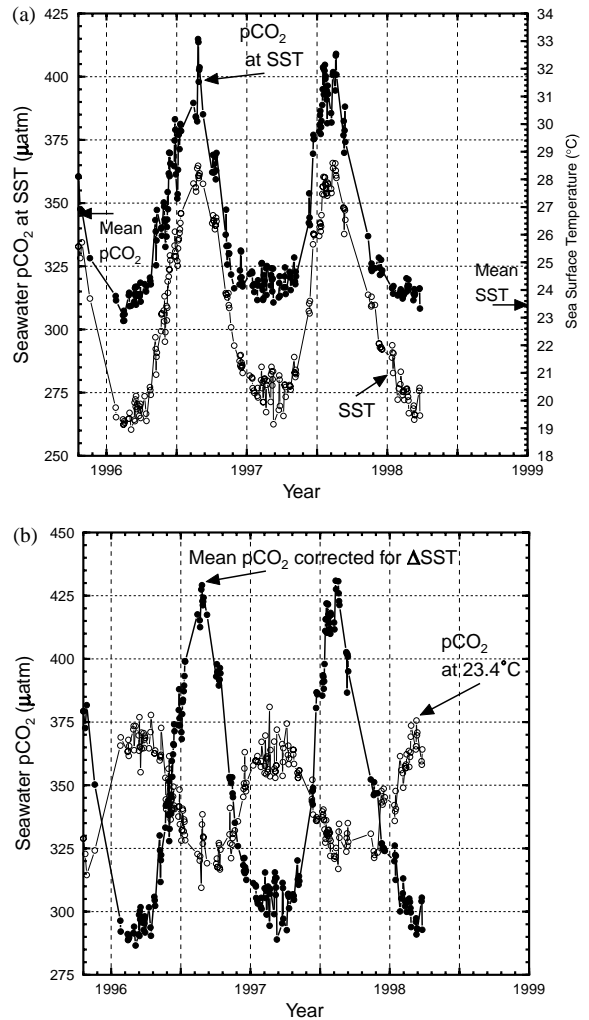


Fig. 3. (A) The surface-water $p\text{CO}_2$ (filled circles) and the temperature of mixed-layer water (SST, open circles) observed at and near the BATS station in 1996 through early 1998. (B) The $p\text{CO}_2$ values at the mean water temperature of 23.4°C (open circles) and the annual mean $p\text{CO}_2$ value corrected for changes in temperature (filled circles).

4.1.1. Seasonal $p\text{CO}_2$ variation at the BATS site, North Atlantic

Fig. 3A shows the multi-year observations from 1996 through early 1998 for the water temperature and $p\text{CO}_2$ made in mixed-layer waters in the vicinity of the BATS site ($32^\circ 50'\text{N}$ and $64^\circ 10'\text{W}$) near Bermuda (Bates, 2001). The temperature (open circles) and $p\text{CO}_2$ (filled circles) are lowest

in winter (February) and highest in summer (July), and their seasonal changes are closely in phase, suggesting that the change in $p\text{CO}_2$ is primarily governed by the temperature change. The peak-to-peak amplitude of seasonal variation in temperature and $p\text{CO}_2$ is $9.5 (\pm 0.3)^\circ\text{C}$ and $100 (\pm 5) \mu\text{atm}$, respectively, in 1996 and 1997. In order to remove the temperature effect from the observed $p\text{CO}_2$, the observed $p\text{CO}_2$ values are normalized to a constant temperature of 23.4°C , the mean annual temperature of seawater at the station, using the equation

$$(p\text{CO}_2 \text{ at } T_{\text{mean}}) = (p\text{CO}_2)_{\text{obs}} \times \exp[0.0423(T_{\text{mean}} - T_{\text{obs}})], \quad (1)$$

where T is the temperature in $^\circ\text{C}$, and the subscripts “mean” and “obs” indicate the annual average and observed values, respectively. Changes in this quantity represent primarily changes in the total CO_2 concentration. The temperature effect on $p\text{CO}_2$ for isochemical seawater ($\partial \ln p\text{CO}_2 / \partial T$) of $0.0423^\circ\text{C}^{-1}$ was determined experimentally by Takahashi et al. (1993) for a North Atlantic surface-water sample. This is nearly independent of temperature and chemical composition (i.e. alkalinity/total CO_2 ratio) of seawater (Rubin, 2000), and may be considered constant. As shown with the open circles in Fig. 3B, the constant-temperature $p\text{CO}_2$ values decrease by about $55 \mu\text{atm}$ from winter through summer in each of 1996 and 1997. This decrease approximates the “net biology” effect, which includes the effects of the net CO_2 utilization, a small amount of net alkalinity change due to carbonate production and nitrate utilization, sea–air exchange of CO_2 , and an addition of CO_2 and alkalinity by the vertical mixing of subsurface waters. However, from winter to summer, the mixed-layer depth tends to become shallower with progressing season, and hence the vertical transport of subsurface waters is considered small. The sea–air gas flux during this period is considered to be small since the sea–air $p\text{CO}_2$ difference changes from positive to negative about midway during the warming period and has a similar magnitude. Bates (2001) observed that, on the average, the total CO_2 concentration in mixed-layer waters decreased from winter to summer by about

$33 \mu\text{mol kg}^{-1}$ (normalized to a constant salinity of 36.6) in both of these years, while the salinity-normalized alkalinity values stayed nearly constant. Using a Revelle factor of 10, the observed seasonal decrease in TCO_2 can be translated to a $p\text{CO}_2$ change of about $60 \mu\text{atm}$. Hence, considering minor changes in the alkalinity, the observed winter-to-summer drawdown of TCO_2 is consistent with the net biological effect estimated using the constant-temperature $p\text{CO}_2$ values.

The effect of temperature changes on $p\text{CO}_2$ has been computed by perturbing the mean annual $p\text{CO}_2$ of $346 \mu\text{atm}$ with the difference between the mean and observed temperature. The $p\text{CO}_2$ value at a given observed temperature, T_{obs} , has been computed using the equation

$$(p\text{CO}_2 \text{ at } T_{\text{obs}}) = (\text{Mean annual } p\text{CO}_2) \exp[0.0423(T_{\text{obs}} - T_{\text{mean}})], \quad (2)$$

where the mean annual temperature, T_{mean} , of 23.4°C is used. The resulting values, that are shown in Fig. 3B with filled circles, indicate the $p\text{CO}_2$ values that would be expected only from temperature changes, if a parcel of water having the mean $p\text{CO}_2$ value of $346 \mu\text{atm}$ is subjected to seasonal temperature changes under isochemical conditions. A mean seasonal amplitude of about $150 \mu\text{atm}$ is observed in 1996 and 1997. This suggests that the increasing effect of winter-to-summer warming on the seawater $p\text{CO}_2$ ($150 \mu\text{atm}$) is partially compensated by the lowering effect of biological utilization of CO_2 ($55 \mu\text{atm}$) to yield the observed seasonal $p\text{CO}_2$ amplitude of $100 \mu\text{atm}$. The relative importance of the temperature and biological effects may be expressed in terms of the ratio, (temperature effect)/(biology effect) or difference [(temperature effect)–(biology effect)]. At this station, the ratio is estimated to be 2.7 (= $150/55 \mu\text{atm}$), and the difference is $+95 \mu\text{atm}$.

4.1.2. Seasonal $p\text{CO}_2$ variation in the Ross Sea, Antarctica

Fig. 4 shows the seasonal variation of surface-water $p\text{CO}_2$ observed during the US JGOFS program in 1996–1998, along the 76.5°S latitude between 169°E and 177°W in the southern Ross Sea, Antarctica. The observations were made from

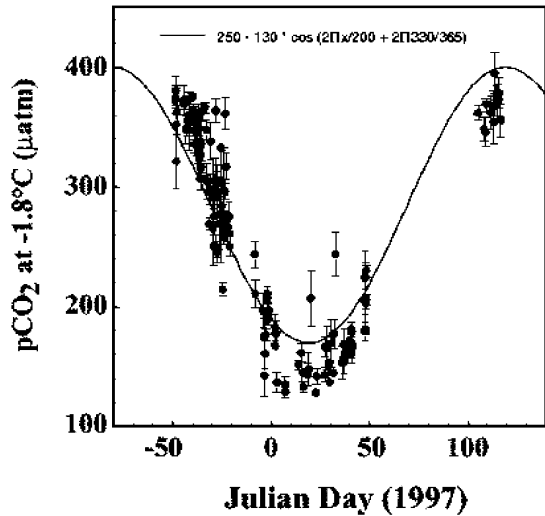


Fig. 4. Seasonal changes in the surface-water $p\text{CO}_2$ observed along 76.5°S in the Ross Sea, Antarctica. Julian date 0 represents January 1, 1997. The solid curve is a trend line approximated by a simple sine function.

November 1996, through the end of February 1997, when the area was not covered with ice (Sweeney, 2000). The seasonal variation is approximated by a sine curve in Fig. 4, showing that the seawater $p\text{CO}_2$ decreases by about $260 \mu\text{atm}$ from about $410 \mu\text{atm}$ in early November to about $150 \mu\text{atm}$ in mid-January. Here, the mixed-layer water temperature is nearly constant ranging between -1.0°C and -1.5°C throughout the open water period, and the effect of temperature on $p\text{CO}_2$ is small (about $5 \mu\text{atm}$). The seasonal variation of $p\text{CO}_2$ is entirely attributed to the biological utilization of CO_2 . Accordingly, the (temperature effect)/(biology effect) ratio is 0.02 ($= 5/260$) or the difference is $-255 \mu\text{atm}$.

4.1.3. Seasonal $p\text{CO}_2$ variation at the Weather Station P, North Pacific

Fig. 5A shows seasonal variations in $p\text{CO}_2$ and temperature observed in mixed-layer waters by Wong and Chan (1991) at the Weather Station “P” in the eastern subarctic Pacific (50°N , 145°W) during 1973–1978. Since their observations have data gaps, the data collected over the 5-year period are plotted for a single year to give a composite

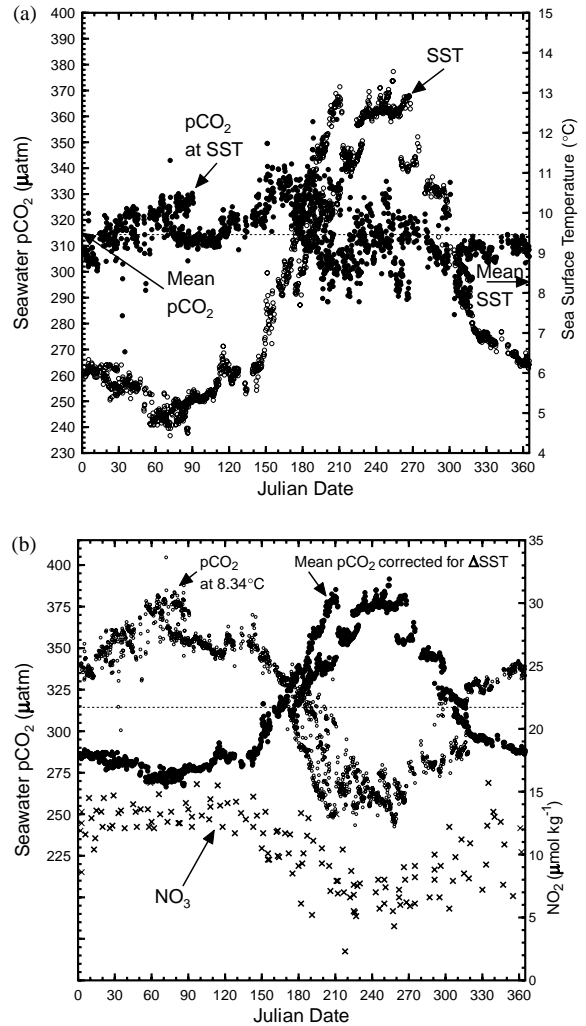


Fig. 5. (A) The $p\text{CO}_2$ and water temperature observed in the mixed layer observed in 1972–1975 at Weather Station “P” by Wong and Chan (1991) are shown with filled and open circles respectively. The multi-year observations are plotted in a single year in order to show a complete annual cycle. (B) The $p\text{CO}_2$ values normalized to the mean annual temperature of 8.34°C are shown with open circles, and the mean annual $p\text{CO}_2$ values corrected for temperature changes are shown with filled circles. The concentrations of nitrate observed at this station by Parslow (1981) are shown with “x”.

seasonal cycle. While the temperature changed seasonally from about 4.5°C to 13°C in a sinusoidal pattern with a spring minimum and a summer maximum, the observed $p\text{CO}_2$ values at in situ temperatures exhibit irregular variations

(three maxima and three minima in a year) fluctuating between 290 and 340 μatm . The $p\text{CO}_2$ values observed at this station exhibit not only much smaller seasonal amplitudes, but also more complex patterns compared to those observed at the BATS station (Fig. 3A). In order to differentiate the effect of biology from that of temperature change, we have computed the $p\text{CO}_2$ values at a mean annual temperature of 8.34°C (open circles, Fig. 5B) using Eq. (1). The biological effect estimated from the temperature normalization is about 115 μatm (375 μatm in February and 260 μatm in July–August, Fig. 5B), twice as large as that observed near Bermuda. At this location, Parslow (1981) has observed a nitrate drawdown of about 8 $\mu\text{mol kg}^{-1}$ (see the “x” symbols in Fig. 3B) from March through July. Assuming the Redfield C/N ratio of 106/15 and the Revelle factor ($\partial \ln p\text{CO}_2 / \partial \ln \text{TCO}_2$) of 12, this nitrate drawdown corresponds to a TCO_2 drawdown of 56.5 $\mu\text{mol kg}^{-1}$ and a $p\text{CO}_2$ decrease of 115 μatm . Thus the magnitude of the biological effect estimated on the basis of the constant-temperature $p\text{CO}_2$ values is consistent with the net biological utilization of CO_2 estimated on the basis of the seasonal drawdown of nitrate. Since the biological drawdown of $p\text{CO}_2$ occurs mostly during the period when the mixed layer is getting shallower with progressing season, the vertical transport contribution of CO_2 -rich subsurface waters is considered minimal.

Fig. 5B shows that the seasonal warming of water causes $p\text{CO}_2$ to increase by about 105 μatm from about 270 μatm in February to 375 μatm in July–August. Thus, the temperature effect is similar in magnitude to the biological effect, but they are approximately 6 months out of phase as photosynthesis is increased at warmer temperatures (Fig. 5B). Hence, at this station, they partially cancel each other, so that the seasonal variation of surface-water $p\text{CO}_2$ is reduced in amplitude without simple sinusoidal seasonal variations. The temperature/biology effect ratio and difference in the effects at this site are, respectively, about 0.9 ($=10/115 \mu\text{atm}$) and $-10 \mu\text{atm}$.

Using the method described above, global-ocean maps showing the respective effects of temperature

and biology on the surface-water $p\text{CO}_2$ and the ratio or difference of these two competing effects may be constructed. The effect of biology on the surface-water $p\text{CO}_2$ in a given pixel area, $(\Delta p\text{CO}_2)_{\text{bio}}$, is represented by the seasonal amplitude of $p\text{CO}_2$ values corrected to the mean annual temperature in a given area, ($p\text{CO}_2$ at T_{mean}), using Eq. (1)

$$(\Delta p\text{CO}_2)_{\text{bio}} = (p\text{CO}_2 \text{ at } T_{\text{mean}})_{\text{max}} - (p\text{CO}_2 \text{ at } T_{\text{mean}})_{\text{min}}, \quad (3)$$

where the subscripts “max” and “min” indicate the seasonal maximum and minimum values.

The effect of temperature changes on the mean annual $p\text{CO}_2$ value, $(\Delta p\text{CO}_2)_{\text{temp}}$, is represented by the seasonal amplitude of ($p\text{CO}_2$ at T_{obs}) values computed using Eq. (2)

$$(\Delta p\text{CO}_2)_{\text{temp}} = (p\text{CO}_2 \text{ at } T_{\text{obs}})_{\text{max}} - (p\text{CO}_2 \text{ at } T_{\text{obs}})_{\text{min}}. \quad (4)$$

The relative importance of the biology and temperature effects is expressed by the ratio, T/B , or the difference ($T - B$):

$$(T/B) = (\Delta p\text{CO}_2)_{\text{temp}} / (\Delta p\text{CO}_2)_{\text{bio}} \text{ or} \\ (T - B) = (\Delta p\text{CO}_2)_{\text{temp}} - (\Delta p\text{CO}_2)_{\text{bio}}. \quad (5)$$

In oceanic areas where the effect of temperature changes on surface-water $p\text{CO}_2$ exceeds the biological effect (e.g., BATS site), the (T/B) ratio is greater than 1 or $(T - B)$ positive, whereas in areas where the biology effect exceeds the temperature effect, the (T/B) ratio varies from 0 to 1 or $(T - B)$ is negative. The two effects cancel each other in areas where the (T/B) ratio is 1 or $(T - B)$ is 0.

4.2. Global distribution of seasonal $p\text{CO}_2$ amplitude

The magnitude of seasonal amplitude has been computed by taking the difference between the maximum and minimum mean monthly surface-water $p\text{CO}_2$ values in each pixel area (Fig. 6). In order to express phase differences in seasonal changes, the following sign conventions are used. When a $p\text{CO}_2$ maximum is found during the period for SST below the annual mean (i.e. colder seasons, or winter), the seasonal amplitude for

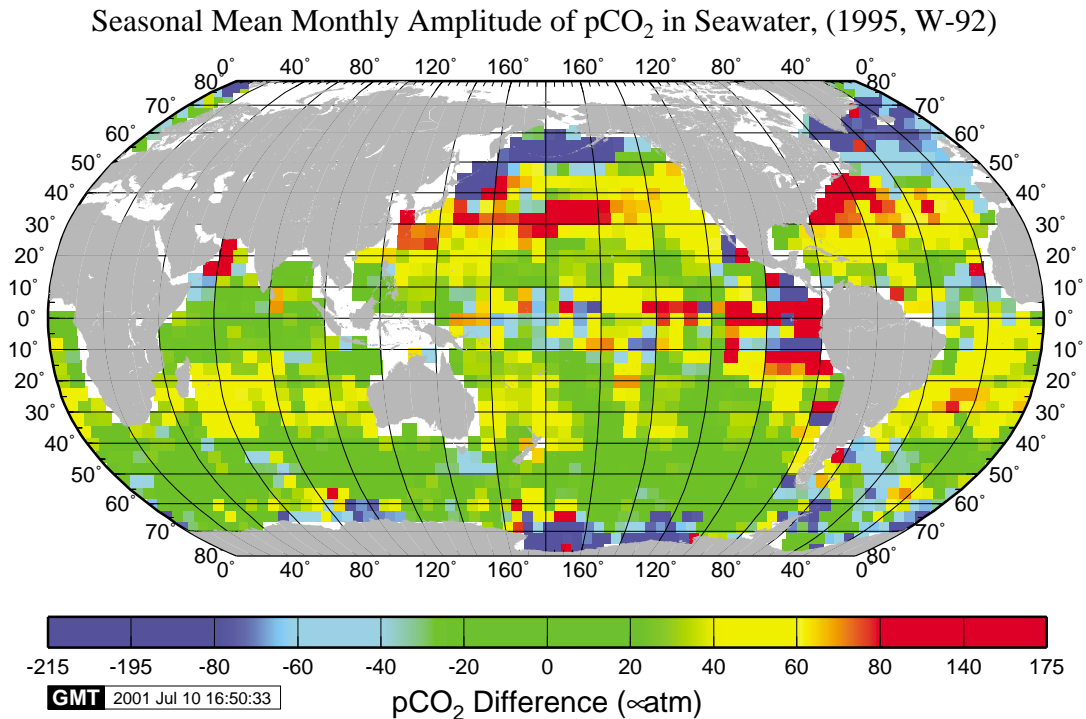


Fig. 6. Distribution of the peak-to-peak seasonal amplitude of surface-water $p\text{CO}_2$. The positive values indicate areas where the surface-water $p\text{CO}_2$ maximum occurs during warm-water seasons, and the negative values indicate areas where $p\text{CO}_2$ maximum occurs during cold-water seasons. Within each hemisphere, seasonal changes for the temperate oceans (positive values) are approximately 6 months out of phase from those (negative values) for the subpolar and polar oceans. The seasonal variation in the northern hemisphere is about 6 months out of phase from that in the southern hemisphere. In several pixels in the subarctic Atlantic, eastern equatorial Pacific, Arabian Sea, Chilean coast, and Antarctic coast, abrupt changes in the signs and colors (from red to dark blue) are observed. Because of the coarse spatial resolution of our analysis, the $p\text{CO}_2$ -SST relations become reversed in areas with fine-scale oceanographic features such as the East Greenland Current in the subarctic Atlantic, the Brazil Current in the South Atlantic and coastal upwelling areas.

$p\text{CO}_2$ is expressed by (minimum–maximum), a negative value. On the other hand, when a $p\text{CO}_2$ maximum is found during the warmer seasons (or summer), the amplitude is expressed by (maximum–minimum), a positive value. This convention has an advantage that differences in timing of seasonal changes within each hemisphere are depicted by the positive (red–yellow) and negative (blue–purple) values. According to this sign convention, the magnitude of amplitude (and colors) observed in the northern oceans can be compared with that (or the same colors) for the southern oceans. However, they are, in fact, about 6 months out of phase.

In Fig. 6, seasonal amplitudes as negative as $-215 \mu\text{atm}$ (blue–purple) are observed in subpolar

and polar regions. This is a result of the biological drawdown of $p\text{CO}_2$ during summer and the increase in $p\text{CO}_2$ during winter due to the vertical mixing of high- CO_2 subsurface waters. The positive values (yellow and red) are found in the mid-latitude oceans where the warm period $p\text{CO}_2$ values are greater than the cold period values. Seasonal amplitudes as large as $120 \mu\text{atm}$ ($282 \mu\text{atm}$ in March and $403 \mu\text{atm}$ in August) are observed in the mid-latitude areas. These are the areas where seasonal temperature changes account for more than 50% of the seasonal $p\text{CO}_2$ changes. The Arabian Sea is an exception to the mid-latitude seasonality, and seasonal amplitudes as large as $174 \mu\text{atm}$ are observed. Here, the minimum monthly $p\text{CO}_2$ value of $355 \mu\text{atm}$ is observed

during March; and the maximum monthly $p\text{CO}_2$ of $529\ \mu\text{atm}$ occurs in July, during which a maximum daily value as high as $640\ \mu\text{atm}$ is observed. The extremely high values are due primarily to the monsoon-induced upwelling of deep waters. Large seasonal amplitudes are also observed near the Chilean coast, where strong upwelling is known to occur. The green areas where seasonal changes are small are found along the boundary between the warm subtropical waters and the colder subpolar waters of the Southern Ocean. This is due to the near cancellation of the temperature effect by the biology effect.

4.3. Distribution of the biological effects on surface-water $p\text{CO}_2$

The global distribution of the biological effect on surface-water $p\text{CO}_2$ (Fig. 7) has been calculated

using Eq. (3). Very large biological drawdown effects on $p\text{CO}_2$ exceeding $140\ \mu\text{atm}$ (yellow–red) are observed in high-latitude northern oceans north of about 40°N (yellow–orange–red). The effects are especially intense in the northwestern subarctic Pacific, where the effects as intense as $264\ \mu\text{atm}$ are observed. The subtropical and tropical oceans in both hemispheres exhibit a small biological drawdown smaller than $50\ \mu\text{atm}$ (light–dark blue). The eastern equatorial Pacific, however, shows intense biological effects up to $276\ \mu\text{atm}$. Moderate to large biological effects ranging from 75 to $120\ \mu\text{atm}$ are seen in the southern hemisphere oceans between 30°S and 50°S . The effect tends to decrease to higher-latitude areas in the Southern Oceans, although locally strong drawdown areas (such as the Ross Sea) are observed.

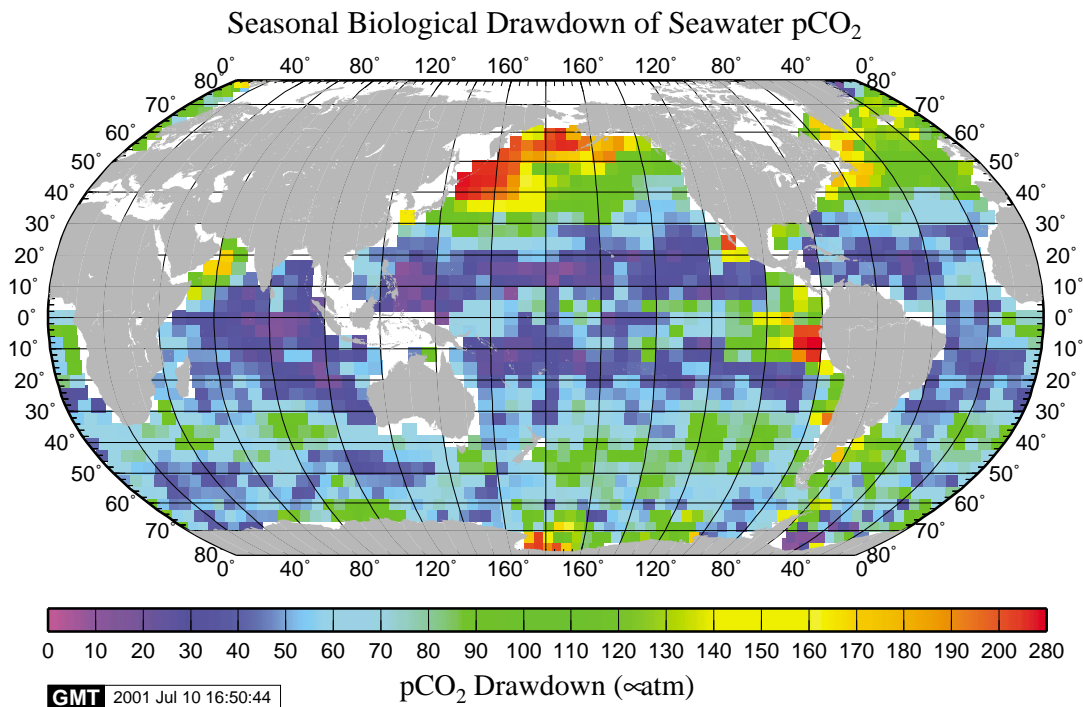


Fig. 7. The effect of the biological utilization of CO_2 is represented by the seasonal amplitude for the $p\text{CO}_2$ values corrected to the mean water temperature for each pixel area using Eq. (3). Values exceeding $150\ \mu\text{atm}$ (yellow–orange–red) are observed in the northwestern subarctic Pacific and Atlantic, the eastern equatorial Pacific, the northwestern Arabian Sea, and the Ross Sea. These high biology areas are associated with intense upwelling of subsurface waters with high CO_2 and nutrient concentrations. Small areas near the coasts of Mexico, Chile and Argentina also show strong biological drawdown effects. We have, however, insufficient seasonal data to characterize the seasonal changes in the southern Weddell Sea and the coastal upwelling areas off West Africa.

We observe that the oligotrophic subtropical gyre areas between 30°N and 30°S (but excluding the 10°N–10°S equatorial Pacific belt and the upwelling areas located in the eastern tropical Pacific and Atlantic and in the Arabian Sea) have an average biological $p\text{CO}_2$ drawdown of about 35 μatm (Fig. 7), whereas the concentrations of nutrients are very low throughout the year with negligibly small seasonal changes. The $p\text{CO}_2$ drawdown corresponds to a TCO_2 decrease of about 20 $\mu\text{mol kg}^{-1}$ that occurred between winter and early summer time when the $p\text{CO}_2$ in seawater becomes minimum. The sea–air CO_2 flux over the oligotrophic waters during the growth period is small as seen in Fig. 2 and may be neglected. Using a mean mixed-layer depth of 50 m (World Ocean Database, 1998), the net biological CO_2 utilization in the mixed layer is estimated to be about 1 mole C m^{-2} for the growth period during which water is warming and mixed-layer depth becomes shallower with the progressing of the season from spring to summer. This is a minimum estimate since the effect of TCO_2 addition by upwelling is neglected. Since this represents early growths over the first 6 months in a year, the annual production may be close to 2 mole $\text{C m}^{-2}\text{yr}^{-1}$. This may be compared with the annual export production for the global oligotrophic ocean estimated by Laws et al. (2000) based upon the SeaWiFS ocean-color data, the vertically generalized production model (VGPM) of Behrenfeld and Falkowski (1997) and a pelagic food web model. Their PTE (primary production and temperature) model solutions give a mean export production (which is assumed to be equal to the new production) of about 20 g $\text{C m}^{-2}\text{yr}^{-1}$ (or 1.7 mole $\text{C m}^{-2}\text{yr}^{-1}$) for the oligotrophic oceans in both hemispheres. Thus, these net production values estimated using independent methods are consistent with each other.

4.4. Distribution of the temperature effect on $p\text{CO}_2$

The effect of seasonal temperature changes on surface-water $p\text{CO}_2$ is calculated using Eq. (4) and the World Ocean Database (1998) SST data recast onto our $4^\circ \times 5^\circ$ grid. The seasonal amplitude is shown in Fig. 8 to depict the global distribution of

the effect on surface-water $p\text{CO}_2$ of seasonal changes in SST. The tropical oceans between 20°N and 20°S have small seasonal temperature changes, and hence small temperature effects on $p\text{CO}_2$ (purple areas). The eastern equatorial areas of the Pacific and Atlantic Oceans are exceptions due to seasonal upwelling of deep waters. The southern high-latitude areas south of about 55°S also show small temperature effects. Large temperature effects exceeding 80 μatm are observed in the mid-latitude areas in both hemispheres. The largest temperature effects, as large as 217 μatm , are observed in the confluence areas of the warm Kuroshio with the cold Oyashio current waters in the northwestern Pacific and of the warm Gulf Stream with the cold Labrador Current waters in the northwestern Atlantic. As shown in Fig. 7, these areas coincide with strong biological effect areas. Since the temperature and biological effects are out of phase in these areas, they tend to cancel each other. However, in the northwestern Pacific, the biology effect exceeds the temperature effect, whereas in the northwestern Atlantic, the temperature effect exceeds the biology effect (see Fig. 9).

4.5. Relative importance of the temperature and biology effects

Fig. 9 shows the global distribution of the difference between the temperature and biology effects ($T - B$) on surface-water $p\text{CO}_2$ computed using Eq. (5). The areas dominated by the biology effect are indicated with green–blue (negative values); and those dominated by the temperature effect are indicated with yellow–orange (positive values). In general, the biology effect dominates the temperature effects in high-latitude oceans in both hemispheres. The equatorial oceans are also dominated by the biology effect. In temperate oceans of both hemispheres, the temperature effect exceeds the biology effect. Along the poleward edge and equatorward edge of the subtropical region, the ($T - B$) becomes nearly zero (green–yellow boundary). This indicates that the effect of temperature cancels with the effect of temperature, and hence that seasonal amplitude of

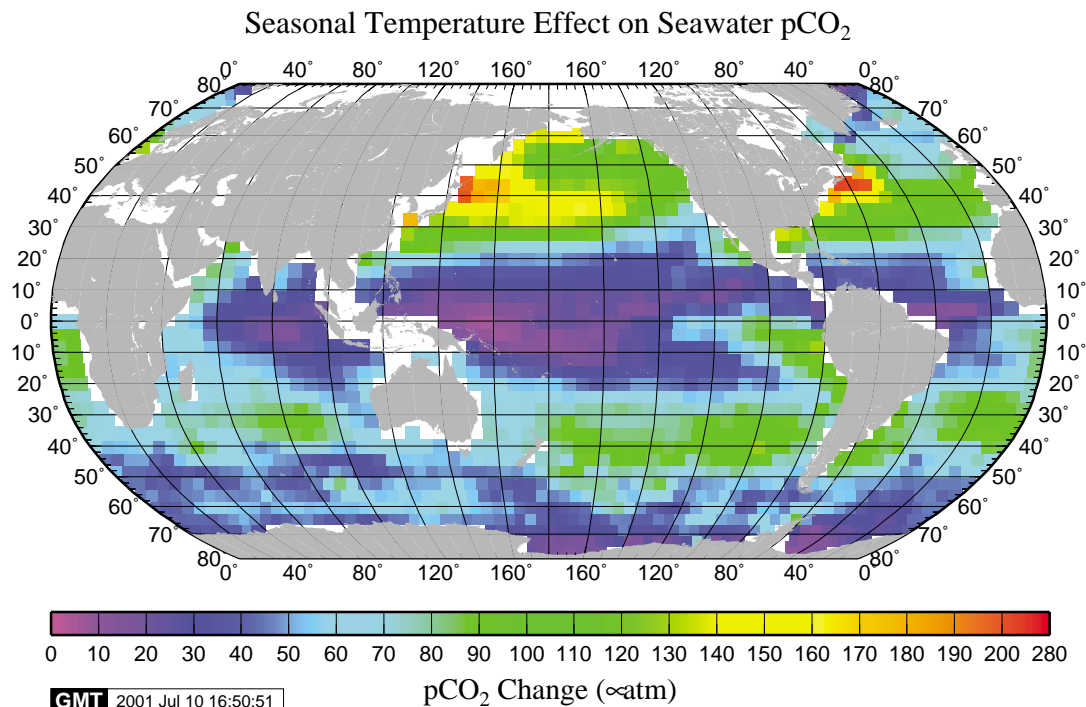


Fig. 8. The effect of seasonal temperature changes on surface-water $p\text{CO}_2$. This is represented by the seasonal amplitude of the mean annual $p\text{CO}_2$ values corrected for seasonal water temperature changes in each pixel area using Eq. (4).

surface-water $p\text{CO}_2$ is small along the transition areas between yellow and green.

Large areas between 40°S and 70°S in the Southern Ocean have negative values (green) indicating that the biology effect exceeds the temperature effect. This feature is demonstrated by the extensive $p\text{CO}_2$ data obtained between 40°S and 65°S during different seasons in the Atlantic, Indian and Pacific sectors of the Southern Ocean under the French KERFIX/F-JGOFS, Australian WOCE and US AESOPS and WOCE programs. The biology effect intensifies to the south, especially in the areas south of the polar front (located about 60°S) and the shelf areas of Antarctica. This suggests that the photosynthetic drawdown of CO_2 in the open Southern Ocean waters, as well as the shelf waters around Antarctica, plays an important role for the transport of atmospheric CO_2 into the deep ocean regime via the thermohaline circulation process.

5. Summary and conclusions

On the basis of about 940,000 surface-water $p\text{CO}_2$ observations, monthly maps showing the climatological distribution and seasonal amplitude for surface-water $p\text{CO}_2$ over the global ocean representing non-El Niño conditions have been constructed for a reference year 1995 with a $4^\circ \times 5^\circ$ spatial resolution. The net sea-air CO_2 flux over the regional and global sea-air ocean has been computed using the NCEP/NCAR 41-year mean monthly wind speeds and the (wind speed)² dependence of sea-air CO_2 gas transfer velocity by Wanninkhof (1992) for long-term wind. A net CO_2 uptake flux by the global oceans of 2.2 Pg C yr^{-1} is obtained. This uptake flux is consistent within $\pm 0.2 \text{ Pg C yr}^{-1}$ with the distribution of the sea-air $p\text{CO}_2$ difference obtained previously using 250,000 (Takahashi et al., 1997) and 550,000 (Takahashi et al., 1999) measurements. Based

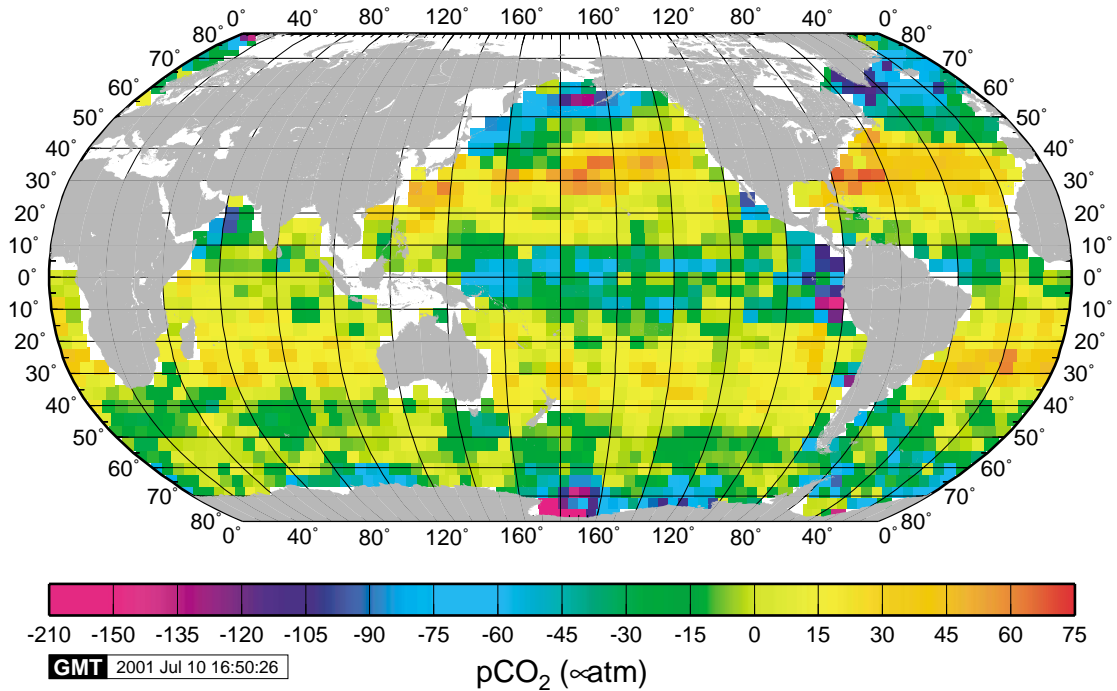


Fig. 9. The difference ($T - B$) between the effects on $p\text{CO}_2$ of seasonal temperature changes and biology. The yellow–orange areas (positive values) are where the temperature effects exceed that of the biological utilization of CO_2 ; the green–blue areas (negative values) are where the biological effect dominates the seasonal changes in surface-water $p\text{CO}_2$.

upon one standard deviation of mean monthly wind speeds over each pixel area, the errors associated with wind-speed variability have been estimated to be about $\pm 20\%$ of the mean annual flux. This estimate for the global-ocean uptake flux is consistent with the values of $2.0 \pm 0.6 \text{ Pg C yr}^{-1}$ estimated on the basis of the observed changes in the atmospheric CO_2 and oxygen concentrations during the 1990s (Keeling et al., 1996; Battle et al., 2000). The CO_2 flux obtained by the present study depends on the relationship between wind speed on sea–air CO_2 gas transfer velocity used for the flux computation. If the (wind speed)³ dependence of Wanninkhof and McGillis (1999) for long-term wind is chosen, the annual ocean uptake as well as the sensitivity to wind variability would be increased by about 70%. The global-ocean uptake flux of 3.7 Pg C yr^{-1} estimated using the (wind speed)³ relation with a Rayleigh wind spectrum is significantly greater than the fluxes estimated from the atmospheric CO_2 and oxygen data.

An ocean zone between 40° and 60° in latitudes in both northern and southern hemispheres is a major sink for atmospheric CO_2 (see Fig. 2). In these areas, poleward-flowing warm waters are in contact and mix with the subpolar waters rich in nutrients. The $p\text{CO}_2$ in surface waters is decreased by the juxtaposition of the cooling effect of warm waters with the biological drawdown effect on $p\text{CO}_2$ in subpolar waters. High wind speeds over these low $p\text{CO}_2$ waters increase the CO_2 uptake rate by ocean waters.

The seasonal amplitude of surface-water $p\text{CO}_2$ at a given location is regulated by the biological utilization of CO_2 and temperature, while the seasonal maximum $p\text{CO}_2$ is governed by the upward flux of high- CO_2 subsurface waters and temperature. In this paper, only the effects of the net biological utilization and seasonal temperature changes on surface-water $p\text{CO}_2$ are discussed. The seasonal amplitude (as defined by the difference between the maximum and minimum values in

monthly mean $p\text{CO}_2$) is as large as $+120\ \mu\text{atm}$ in temperate oceans and $-215\ \mu\text{atm}$ in the polar oceans. The sign change indicates that the seasonality in the subpolar and polar areas is approximately 6 months out of phase from that in the temperate and tropical ocean areas. Because of this phase difference, a zone of near-zero seasonal amplitude is formed when the amplitudes for these effects are nearly equal but opposite in the seasonal phase. Such a zone is found along the poleward and equatorward borders of subtropical gyres as indicated by the yellow–green color transition in Fig. 9.

Combining the surface-ocean $p\text{CO}_2$ data with the climatological SST data, the biological component in seasonal $p\text{CO}_2$ changes is separated from the temperature change component, and the relative importance of these two effects is presented. The biological component is estimated by the seasonal amplitude of the temperature-normalized $p\text{CO}_2$ values. The temperature component is characterized by the seasonal amplitude of the annual mean $p\text{CO}_2$ value in a given area corrected for seasonal temperature variation. The global maps showing each of these components and their relative importance are presented. The seasonal changes in the following areas are found to be strongly controlled by the biological processes; the equatorial and subpolar–polar oceans, the northwestern Arabian Sea, the eastern equatorial Pacific, the upwelling area off the Chile coast, the subarctic northwestern Pacific, the subarctic North Atlantic and the coastal waters around Antarctica (including the Ross Sea). On the other hand, in the subtropical gyre areas, the effect of temperature change exceed the biological effect by as much as $60\ \mu\text{atm}$ or a factor of 4. Although the biological effect is small in these areas, it is about $35\ \mu\text{atm}$ on the average over the oligotrophic waters (10°N – 30°N and 10°S – 30°S). This $p\text{CO}_2$ effect is equivalent with a biological CO_2 utilization of $20\ \mu\text{mol CO}_2\ \text{kg}^{-1}$ for a period from winter through the spring growth period, and is broadly consistent with the export production estimated by Laws et al. (2000) using the SeaWiFS data.

The climatological $p\text{CO}_2$ data presented in this paper show the importance of high-latitude northern and southern oceans as a sink for atmospheric

CO_2 . These areas are also the source areas for the deep and intermediate water masses and hence represent a direct pathway for CO_2 exchange between the atmosphere and deep oceans. Therefore, the mechanisms that control the sea–air CO_2 flux and the CO_2 concentration in newly formed waters must be understood in order to predict the long term storage of CO_2 in deep ocean waters. We need to understand the oceanic biogeochemical feedback processes in response to the anthropogenic loading of atmospheric CO_2 as well as changes in the climate and associated changes in ocean ecology and biogeochemistry (e.g., Karl, 1999). The findings of this study should serve as a basis for characterizing future changes in the oceanic CO_2 uptake.

The monthly $p\text{CO}_2$ values and other values presented in this paper are available in an electronic format at a FTP site at the Lamont–Doherty Earth Observatory of Columbia University via an e-mail address <taka@ldeo.columbia.edu>.

Acknowledgements

This study was made possible by international collaboration of field measurements of surface-water $p\text{CO}_2$ obtained over many years. We gratefully acknowledge the financial support offered to us by various government agencies in Australia, France, Iceland, Japan and the United States (National Science Foundation, National Oceanographic and Atmospheric Administration and Department of Energy). The database construction and data analysis have been supported by grants from the US National Oceanographic and Atmospheric Administration. We thank for the encouragements and assistance offered by Paul Treguer, Chairman of the Southern Ocean CO_2 Symposium held in Brest, France, during the preparation of this paper. This is Contribution No. 6226 of LDEO.

References

- Atlas of Surface Marine Data, 1994. CD-ROM NODC-56, Ocean Climate Laboratory, NOAA, Washington, DC.

- Bates, N.R., 2001. Interannual variability of oceanic CO₂ and biogeochemical properties in the Western North Atlantic subtropical gyre. *Deep-Sea Research II* 48 (8–9), 1507–1528.
- Bates, N.R., Takahashi, T., Chipman, D.W., Knapp, A.H., 1998. Variability of *p*CO₂ on diel to seasonal time scales in the Sargasso Sea. *Journal of Geophysical Research* 103, 15567–15585.
- Battle, M., Bender, M.L., Tans, P.P., White, J.W.C., Ellis, J.T., Conway, T., Francey, R.J., 2000. Global carbon sinks and their variability inferred from atmospheric O₂ and δ¹³C. *Science* 287, 2467–2470.
- Behrenfeld, M.J., Falkowski, P.G., 1997. Photosynthetic rates derived from satellite-based chlorophyll concentration. *Limnology and Oceanography* 42, 1–20.
- Etcheto, J., Boutin, J., Dandonneau, Y., Bakker, D.C.E., Feely, R.A., Ling, R.D., Nightingale, P.D., Wanninkhof, R., 1999. Air–sea CO₂ flux variability in the equatorial Pacific Ocean near 110°W. *Tellus* 51B, 734–747.
- Feely, R.A., Wanninkhof, R., Takahashi, T., Tans, P., 1999. Influence of El Niño on the Equatorial Pacific contribution to atmospheric CO₂ accounts. *Nature* 398, 597–601.
- GLOBALVIEW-CO₂: Cooperative Atmospheric Data Integration Project—Carbon Dioxide, 2000. CD-ROM, NOAA CMDL, Boulder, CO. Also available on Internet via anonymous FTP to <ftp.cmdl.noaa.gov>, Path: <cgc/co2/GLOBALVIEW>.
- Inoue, H.Y., Matsueda, H., Ishii, M., Fushimi, K., Hirota, M., Asanuma, I., Takasugi, Y., 1995. Long-term trend of the partial pressure of carbon dioxide (*p*CO₂) in surface waters of the western North Pacific 1984–1993. *Tellus* 47B, 391–413.
- Jenkins, W.J., 1991. Determination of isopycnal diffusivity in the Sargasso Sea. *Journal of Physical Oceanography* 21, 1058–1061.
- Joos, F., Bruno, M., 1998. Long-term variability of the terrestrial and oceanic carbon sinks and the budgets of the carbon isotopes ¹³C and ¹⁴C. *Global Biogeochemical Cycles* 12, 277–295.
- Karl, D.M., 1999. A sea of change: biogeochemical variability in the North Pacific subtropical gyre. *Ecosystems* 2, 181–214.
- Keeling, C.D., Whorf, T.P., 2000. Atmospheric CO₂ concentrations—Mauna Loa Observatory, Hawaii, 1958–1999 (revised August 2000). CDIAC NDP-001 (<http://cdiac.esd.ornl.gov/ndps/ndp001.html>), Carbon Dioxide Information and Analysis Center, Oak Ridge, TN.
- Keeling, R., Piper, S.C., Heinmann, M., 1996. Global and hemispheric CO₂ sinks deduced from changes in atmospheric O₂ concentration. *Nature* 381, 218–221.
- Laws, E.A., Falkowski, P.G., Smith Jr., W.O., Ducklow, H., McCarth, J.J., 2000. Temperature effects on export production in the open ocean. *Global Biogeochemical Cycles* 14, 1231–1246.
- Martinson, D.G., 1990. Evolution and the southern Antarctic mixed layer and sea–ice; open ocean deep water formation and ventilation. *Journal of Geophysical Research* 95, 11641–11654.
- Martinson, D.G., Iannuzzi, R.A., 1998. Antarctic ocean–ice interaction: implications from ocean bulk property distributions in the Weddell gyre. *Antarctic Sea Ice Physical Processes, Interactions and Variability*, Antarctic Research Series, Vol. 74. American Geophysical Union, Washington, DC, pp. 243–271.
- Metzl, N., Poisson, A., Louanchi, F., Brunet, C., Schauer, B., Bres, B., 1995. Spatio-temporal distributions of air–sea fluxes of CO₂ in the Indian and Antarctic oceans: a first step. *Tellus* 47B, 56–69.
- Metzl, N., Tilbrook, B., Poisson, A., 1999. The annual fCO₂ cycle and the air–sea CO₂ flux in the sub-Antarctic Ocean. *Tellus* 51B, 849–861.
- Murphy, P.P., Harrison, D.E., Feely, R.A., Takahashi, T.T., Weiss, R.F., Gammon, R.H., 1998. Variability of Δ*p*CO₂ in the subarctic North Pacific: a comparison of results from four expeditions. *Tellus* 50B, 185–204.
- Nojiri, Y., 2001a. Surface water and atmospheric *p*CO₂ data observed aboard the Alligator Hope. Center for Global Environment Research, National Institute for Environmental Studies, Japan, <www.mirc.jha.or.jp/nies/AH>.
- Nojiri, Y., 2001b. Surface water and atmospheric *p*CO₂ data observed aboard the Skaugran. Center for Global Environment Research, National Institute for Environmental Studies, Japan, <www.mirc.jha.or.jp/nies/SK>.
- Parslow, J.S., 1981. Phytoplankton-zooplankton interactions: Data analysis and modelling (with particular reference to Ocean Station P (50°N, 145°W) and controlled ecosystem experiments). Ph.D. Thesis, University of British Columbia.
- Quay, P., 1987. Was a carbon balance measured in the equatorial Pacific? *Deep-Sea Research II* 44, 1765–1782.
- Rubin, S.I., 2000. Processes controlling the distribution of carbon dioxide and nutrients in the South Pacific and Southern Oceans. Ph.D. Thesis, Columbia University, New York, NY, 223pp.
- Rubin, S.I., Takahashi, T., Chipman, D.W., Goddard, J.G., 1998. Primary production and nutrient utilization ratios in the Pacific Sector of the Southern Ocean based on seasonal changes in seawater chemistry. *Deep-Sea Research I* 45, 1211–1234.
- Sabine, C.L., Key, R.M., 1998. Final report for underway surface CO₂ measurements on WOCE Leg P17E/P19S, Technical Report #98-3, Ocean Tracer Laboratory, Department of Geosciences, Princeton University, Princeton, NJ, 13pp.
- Sabine, C.L., Key, R.M., Kozyr, A. (Eds.), 1997. Surface water and atmospheric underway carbon dioxide data obtained during the World Ocean Circulation Experiment Indian Ocean Survey Cruises (R/V Knorr, December 1994–January, 1996), ORNL/CDIAC-103, NDP-064, Carbon Dioxide Information Analysis Center, Oak Ridge National Laboratory, Oak Ridge, TN, 89pp.
- Sabine, C.L., Key, R.M., Hall, M., Kozyr, A. (Eds.), 1999. Carbon dioxide, hydrographic and chemical data obtained during the R/V Thomas G. Thompson cruise in the Pacific Ocean (WOCE section P10, October 5–November 10, 1993). ORNL/CDIAC-122, NDP-071, Carbon Dioxide

- Information Analysis Center, Oak Ridge National Laboratory, US Department of Energy, Oak Ridge, TN, 68pp.
- Sabine, C.L., Wanninkhof, R., Key, R.M., Goyet, C., Millero, F.J., 2000. Seasonal CO₂ fluxes in the tropical and subtropical Indian Ocean. *Marine Chemistry* 72, 33–55.
- Sarmiento, J.L., Orr, J.C., Siegenthaler, U., 1992. A perturbation simulation of CO₂ uptake in an ocean general circulation model. *Journal of Geophysical Research* 97, 3621–3645.
- Siegenthaler, U., Sarmiento, J.L., 1993. Atmospheric carbon dioxide and the ocean. *Nature* 365, 119–125.
- Sweeney, C., 2000. Biogeochemical regimes and meso-scale variability in the Ross Sea, Antarctica. Ph.D. Thesis, Columbia University, New York, NY, 137pp.
- Sweeney, C., Hansell, D.A., Carlson, C.A., Codispoti, L.A., Gordon, L.I., Marra, J., Millero, F.J., Smith, W.O., Takahashi, T., 2000b. Biogeochemical regimes, net community production and carbon export in the Ross Sea, Antarctica. *Deep-Sea Research II* 47, 3369–3394.
- Sweeney, C., Smith, W.O., Hales, B., Bidigare, R.R., Carlson, C.A., Codispoti, L.A., Gordon, L.I., Hansell, D., Millero, F.J., Park, Mi-OK, Takahashi, T., 2000b. Nutrient and carbon removal ratios and fluxes in the Ross Sea, Antarctica. *Deep-Sea Research II*, 47, 3395–3421.
- Takahashi, T., Goddard, J., 1998. Measurement of the total CO₂ concentration and total alkalinity in seawater collected during the SONNE Cruise 102, May–June, 1985. Final Technical Report, Lamont–Doherty Earth Observatory, Palisades, NY, 54pp.
- Takahashi, T., Olafsson, J., Goddard, J., Chipman, D.W., Sutherland, S.C., 1993. Seasonal variation of CO₂ and nutrients in the high-latitude surface oceans: a comparative study. *Global Biogeochemical Cycles* 7, 843–878.
- Takahashi, T., Takahashi, T.T., Sutherland, S.C., 1995. An assessment of the role of the North Atlantic as a CO₂ sink. *Philosophical Transactions of the Royal Society of London, Series B* 348, 143–152.
- Takahashi, T., Feely, R.A., Weiss, R., Wanninkhof, R.H., Chipman, D.W., Sutherland, S.C., Takahashi, T.T., 1997. Global air–sea flux of CO₂: an estimate based on measurements of sea–air pCO₂ difference. *Proceedings of the National Academy of Science* 94, 8292–8299.
- Takahashi, T., Wanninkhof, R.H., Feely, R.A., Weiss, R.F., Chipman, D.W., Bates, N., Olafsson, J., Sabine, C., Sutherland, S.C., 1999. Net sea–air CO₂ flux over the global oceans: An improved estimate based on the sea–air pCO₂ difference. In: Yukihiro Nojiri (Ed.), *Proceedings of the Second International Symposium, CO₂ in the Oceans* (ISSN 1341-4356), Center for Global Environmental Research, National Institute for Environmental Studies, Tsukuba, Japan, pp. 9–14.
- Takahashi, T., Sweeney, C., Sutherland, S.C., Chipman, D.W., Goddard, J., Rubin, S.I., 2000. Method of underway pCO₂ measurements in surface waters and the atmosphere during the AESOP Expeditions, 1996–1998 in the Pacific sector of the Southern Ocean and the Ross Sea. US JGOFS Data Center, Woods Hole Oceanographic Institution, Woods Hole, MA.
- Thiele, G., Roether, W., Schlosser, P., Kuntz, R., Siedler, G., Stramma, L., 1986. Baroclinic flow and transient-tracer fields in the Canary-Cape Verde Basin. *Journal of Physical Oceanography* 16, 814–826.
- Toggweiler, J.R., Dixon, K., Bryan, K., 1989. Simulations of radiocarbon in a coarse resolution world ocean model I: steady state pre-bomb distributions. *Journal of Geophysical Research* 94, 8217–8242.
- Wanninkhof, R., 1992. Relationship between wind speed and gas exchange. *Journal of Geophysical Research* 97, 7373–7382.
- Wanninkhof, R., McGillis, W.M., 1999. A cubic relationship between gas transfer and wind speed. *Geophysical Research Letters* 26, 1889–1892.
- Wanninkhof, R., Doney, S.C., Takahashi, T., McGillis, W.R. (2002). The effect of using time-averaged winds on regional air–sea CO₂ fluxes. In: Donelan M., Drennan W., Saltzman E., Wanninkhof R. (Eds.), *Gas Transfer at Water Surfaces*, AGU Geophys. Monograph 127, Washington, DC. 351–356.
- Weiss, R.F., 1974. Carbon dioxide in water and seawater: the solubility of a non-ideal gas. *Marine Chemistry* 2, 203–215.
- Wong, C.S., Chan, Y.-H., 1991. Temporal variations in the partial pressure and flux of CO₂ at ocean station P in the subarctic northeast pacific ocean. *Tellus* 43B, 206–223.
- World Ocean Database, 1998. Version 2, the National Oceanographic Data Center, NOAA, Washington, DC.